

Surrogate-Based Optimization of Aircraft Propeller Performance Using A High-Fidelity and Efficient RANS Framework

Arne Stürmer, Martin Hepperle, Patrick Wegener

DLR Institute of Aerodynamics and Flow Technology, Transport Aircraft Branch
Lilienthalplatz 7, 38108 Braunschweig, Germany

Abstract

In the frame of the DLR-self funded PrOpti-project, the DLR Institute of Aerodynamics and Flow Technology is utilizing a surrogate based optimization approach built around a high-fidelity RANS aerodynamic analysis for the multi-disciplinary design of aircraft propeller blades to meet the increasingly challenging requirements for a high propulsive efficiency with low cabin and community noise levels. In a previous collaborative effort with a small aircraft manufacturer, a single-disciplinary, multi-objective framework for the aerodynamic optimization of propellers was developed, which is the baseline for the planned extension to include aeroacoustics in the design loop in PrOpti, and which is the main focus of the work discussed in this paper.

Keywords: Propeller, Aerodynamics, RANS, Optimization, SBO

1. Introduction

The aviation industries push to continuously and aggressively reduce the sectors climate impact is a very challenging goal requiring significant technology improvement and development. Turboprop propulsion, boasting a fuel efficiency benefit of up to 40% versus turbofans, is increasingly becoming an obvious and important technology brick to meet this challenge. The aggressive efficiency requirements set for future new propeller and open rotor propulsion systems, coupled with equally critical limits in terms of the propulsion and overall aircraft cabin and community noise levels demand novel and highly-accurate design approaches to ensure aviation can meet the expectations and necessities of reduced climate and environmental impact as well as acceptance by airlines, passengers and the general public. In the frame of the DLR-self funded PrOpti-project, the DLR Institute of Aerodynamics and Flow Technology is utilizing a surrogate based optimization (SBO) approach built around a high-fidelity RANS (Reynolds Averaged Navier-Stokes) aerodynamic analysis for the multi-disciplinary design of aircraft propeller blades to meet the increasingly challenging requirements for a high propulsive efficiency with low cabin and community noise levels. In a previous collaborative effort with a small aircraft manufacturer, a single-disciplinary, multi-objective framework for the aerodynamic optimization of propellers was developed, which is the baseline for the planned extension to include aeroacoustics in the design loop in PrOpti, and which is the main focus of the work discussed in this paper.

2. Geometry and Test Case Definition

In the frame of the DLR-AS PrOpti project the goal is to develop modern design tools and approaches and utilize and demonstrate these by optimizing a propeller design aimed at being a possible replacement of an existing 6-bladed propeller for an aircraft in the sub-50-seat regional turboprop class. The propeller diameter of D=3.6m is not a design variable and remains constant at this point of the optimization studies. The design goals for the propeller are to achieve notably lower take-off noise emissions, while at least maintaining if not improving the aerodynamic performance across the complete operating range of the aircraft. The engine and aircraft operating points for a broad range of the key flight conditions serve as specifications to guide the design process, with the design cruise point, for example, specifying the engine shaft power and required propeller thrust for flight of just

under M=0.5 at 20000ft, and a similar data set defining the requirements for a take-off condition of M=0.2 at 750ft of altitude. The three most important operating point specifications are listed for reference in table 1, with the cruise and take-off cases being the main focus in the work discussed in this paper.

Operating Point	Altitude h [ft]	Mach M [-]	Advance Ratio J [-]	Thrust Coefficient C_T, [-]	Power Coefficient C_P, [-]
Take-Off, MT2	750	0.2	0.869	0.203	0.224
Cruise, CR3	20000	0.5	2.506	0.181	0.517
Climb, CL5	25000	0.4	1.932	0.196	0.435

Table 1: Reference propeller operating point specifications and performance requirements

2.1 Baseline Propeller Blade Design

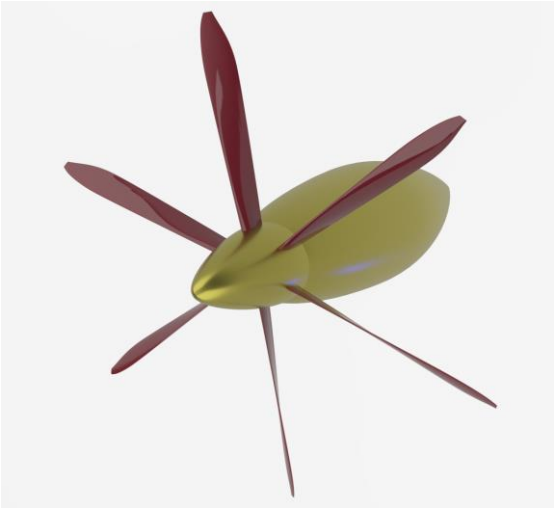


Figure 1 – PROPPY-based baseline propeller design matching the current propeller operating characteristics

The important first step in the project was the conceptual design of a reference propeller as a generic equivalent of the design currently powering the regional turboprop target aircraft. This baseline propeller was created using the inverse design method implemented in the propeller design and analysis code PROPPY in a well-established and proven approach that has been utilized at DLR-AS for countless propeller designs spanning decades. This propeller blade was targeted towards an optimal match of the performance specs at a selected cruise point and then analyzed in selected off-design operating points. The inverse design procedure in PROPPY is based on the classical Prandtl/Betz model for propellers of minimum induced loss. The prescribed distribution of the airfoils and the lift coefficient along the radius defines the blade geometry as chord and twist distributions along the radius. For the subsequent off-design analyses under constant speed operation, the analysis method determines the required blade angle for the desired thrust setting. The final baseline design, as shown in Figure 1, was able to match the reference propeller specs very well for all of the flight conditions under study and served as the generic baseline 6-bladed propeller for the optimization studies.

2.2 RANS-Based Baseline Propeller Performance Analysis

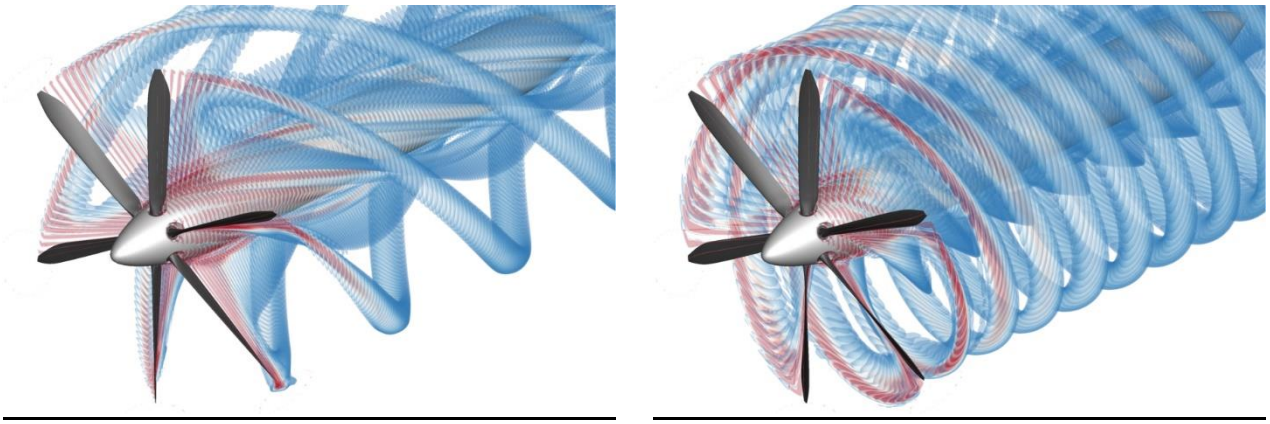


Figure 2 – RANS analysis results, showing propeller tip vortices and blade wakes through vorticity contours, for the baseline propeller at the cruise (left) and take-off (right) operating point

The baseline propeller design from PROPPY was then analyzed across the full operating spectrum using the same RANS-based analysis with the DLR TAU-Code that is a part of the optimization

framework described in the next section. This step is necessary to verify the PROPPY results using the more expensive but higher-fidelity CFD methods on the one hand, and to establish the relevant baseline aero performance levels using the same tools and approaches applied in the optimization. Furthermore, the CFD data is used as input to the aeroacoustic prediction tools, that similarly deliver the baseline reference values against which the optimized propeller noise emission will be evaluated in the future multi-disciplinary extension of this work. RANS simulations were done for a total of 8 key flight conditions, including the 3 primary operating points listed in table 1, with Figure 2 showing sample results for the two most important operating points driving the blade design: cruise and take-off. The RANS results were in very good agreement with the predictions of the conceptual design tools. These CFD results will also serve as restart solutions for each subsequent blade optimization cycle, helping to notably reduce RANS turn-around times.

3. SMARTy-Based Process Chain for the Aerodynamic Performance SBO of Propellers

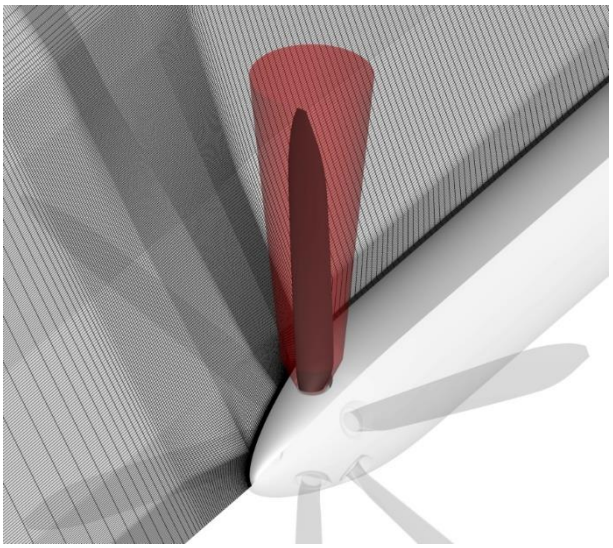


Figure 3 – RANS mesh setup with an embedded blade mesh block for the runtime adjustment of the blade pitch angle

The RANS CFD simulations are performed utilizing the DLR TAU-Code, building on a body of know-how and successful applications to many propeller and open rotor investigations [1–5]. The DLR TAU-code [6] is an unstructured finite-volume vertex-based CFD solver developed by DLR. For the simulations described here, spatial discretization of the convective fluxes is done using a second order central differencing scheme with scalar dissipation while the viscous fluxes are discretized with central differences. Turbulence in these fully turbulent simulations is modeled with the 1-equation model of Spalart-Allmaras [7]. Time-stepping is handled using a lower-upper symmetric Gauss-Seidel (LU-SGS) implicit relaxation scheme with convergence acceleration through local time stepping, multigrid and residual smoothing [8]. As the most time-consuming step in the high-fidelity optimization of a propeller blade, efficiencies to speed up the RANS analysis are a key enabler to make CFD-based optimization a viable tool in a propeller blade design. For propellers, simplifying the problem to that of an isolated propeller at axial flow is an accepted approach, which allows the aerodynamics performance to be accurately obtained as a steady state flow in the propellers rotating frame of reference. An additional runtime reduction is achieved by making use of the DLR TAU Codes Chimera/Overset mesh capability, as can be seen in Figure 3.

The baseline RANS-based single-disciplinary aerodynamic optimization approach and process chain that was established in a prior project was essentially re-used as the starting point for the planned multi-disciplinary optimization including aeroacoustics planned in PrOpti, adding only some minor refinements to some process steps. Figure 3 sketches the process chain for the single-disciplinary aerodynamic propeller optimization which is the focus in this paper.

Starting point in the RANS simulation chain is a parametric CATIAv5 CAD-Model, that delivers an updated blade shape for each optimization step in an automated process. In the present work, 14 blade planform shape parameters are used, with the blade twist and chord parameterized at 5 radial stations, while 4 airfoil stacking parameters are used for the blade sweep. The blade twist design space allows for a 3 degree increase and decrease of the airfoil pitch angle versus those of the baseline blade at the root, the radial positions of r/R=0.39, 0.59, 0.80 and the tip. The blade chord design space is defined through a scaling factor, which allows for up to a 25% reduction in the airfoil chord versus the baseline blade at r/R=0.18, and a 25% increase and decrease of the section length at radial positions of r/R=0.49, 0.76, 0.94 and the blade tip. Finally, to enable a blade planform shape with a structurally and aeroelastically feasible leading-edge sweep, the airfoils at radial stations of r/R=0.39, 0.59 and 0.80 are allowed a chordwise displacement in leading edge direction of up to 50%

of the respective baseline blade chord lengths, while the tip section can shift by this increment both in the leading and trailing edge direction. The CATIA step is the foundation of the entire process, and significant effort was required to ensure the parametrization is able to yield a near-perfect approximation of the baseline, starting blade shape as well as allow for a robust automatic update of that shape using the 14 planform parameters that enables a broad design space exploration delivering shapes suitable for the subsequent meshing step.

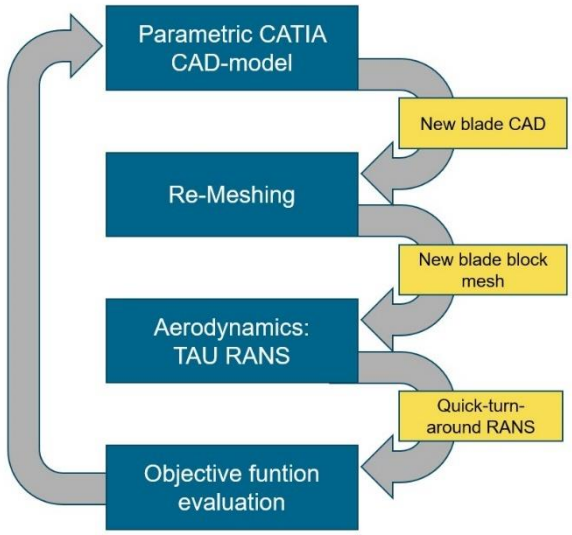


Figure 4 – SMARTy-based framework for the high-fidelity RANS optimization of propellers

Three additional important aspects are also addressed in the CATIA modeling step. First, based on discussions with propeller blade manufacturers, constraints are included, that aim to prohibit blade shapes, which are not feasible in the build process. These include airfoil thicknesses across the radius, the trailing edge thickness and the leading-edge radii for example. And furthermore, the parameter space is carefully chosen to respect basic blade design guidelines to avoid aeroelastically critical shapes, as at present the third key design propeller design discipline, structural mechanics, is not a component of the high-fidelity optimization process chain. Finally, to enable the use of block-structured blade mesh blocks, with significant benefits in terms of the efficiency and speed of the RANS simulation turn-around times, robust helper geometries used to define edges and mesh block boundaries that move in accordance with the blade shape update are also done in the parametric CATIA model.

Each new parameter set in the optimization thus delivers an error-free CAD-model to the next step in the process chain, the blade block remeshing. This is done using the commercial grid generation tool Fidelity Pointwise, driven by the python-based scripting framework RoMeO (Rotor Mesh Optimization) developed and made available for this work by the Wind Energy Department of the institute. For simplicity and robustness, an O-Mesh topology is used to mesh the cylindrical blade mesh block, which ensures a high-quality boundary layer resolution, including the laminar sub-layer, on all blade surfaces is achieved. For each new blade shape, the resulting new blade mesh block is then combined with the existing nacelle mesh, making use of the Chimera/Overset meshing capability available in the DLR TAU-Code.

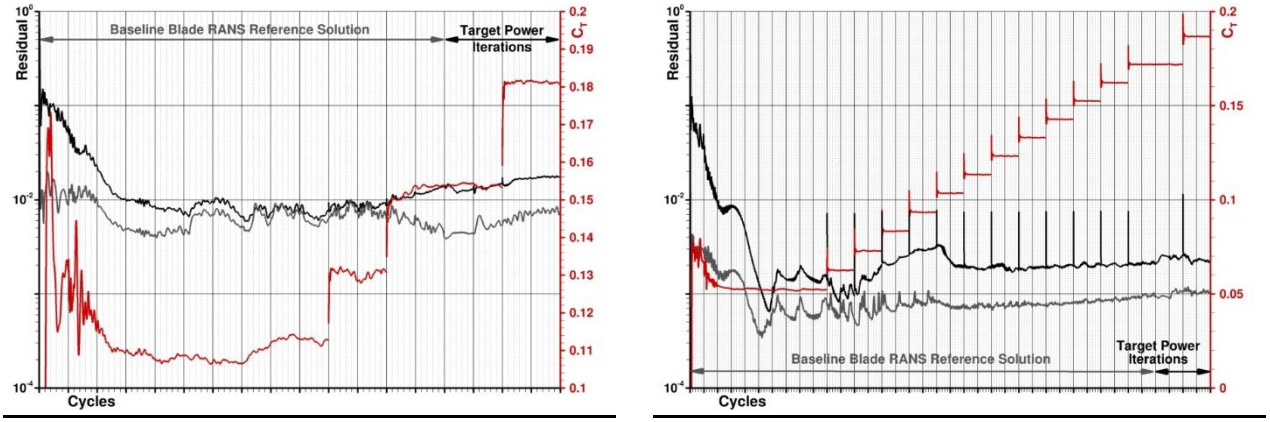


Figure 5 – Sample convergence plots of a target-power RANS analysis cycle based on the Chimera-capabilities in the DLR TAU-Code for the cruise (left) and take-off (right) operating point

As each new blade mesh block is identical in terms of topology and node count to the baseline blade mesh, the subsequent RANS analysis be initiated as a restart from the baseline configuration RANS

solution. For each blade shape and operating point, a python-scripted TAU RANS simulation is run, which uses the Chimera approach to adjust the blade mesh block pitch in an iterative manner to absorb the specified engine shaft power in each case. Figure 5 shows an example convergence plot for the cruise evaluation on the left, and the take-off case on the right. In each figure, a gray arrow marks the portion of the RANS simulation that is run only once for the baseline blade shape. The result of this RANS run can then be used as a restart solution for any subsequent blade shape design iteration int the target-power iteration portion of the simulation. For both operating points, typically between 2 and 3 blade pitch iterations are required to obtain a result at the specified shaft power, for which a tolerance of +/-0.5% versus the operating point specification is set. Of note are the slightly higher amplitude fluctuations in the thrust coefficient values for the cruise case per blade pitch cycle in comparison to a near-perfect constant value seen for the take-off case. This is caused by a more pronounced trailing edge flow separation at the blade foot for the cruise operating point, in the region where the blade transitions from the root airfoil shape to the cylindrical hub intersection. These oscillation manifest also as a noisier signal in the cruise case objective function evaluation, introducing a small increase in uncertainty for this operating point in comparison to the take-off case. An operating point evaluation – with the different points per blade shape able to be run in parallel for multi-objective cases – completing typically in about 2-3 hours.

Factoring in the much shorter runtimes for the previous process steps as well as time required to copy data between the workstations running the CAD and meshing steps and the HPC cluster used for the RANS step, more than 10 design cycles per 24h period can thus be evaluated.

The overall process, including the objective function evaluations, are controlled using a python-scripted SB-optimization loop, drawing on the functionality provided by the SMARTy (Software for data-driven aerodynamic modeling, analysis and design) package, developed and supported in house by the AS-C^{2}A^{2}S^{2}E department of the institute [9,10].

4. Optimization Results and Aerodynamic Analysis

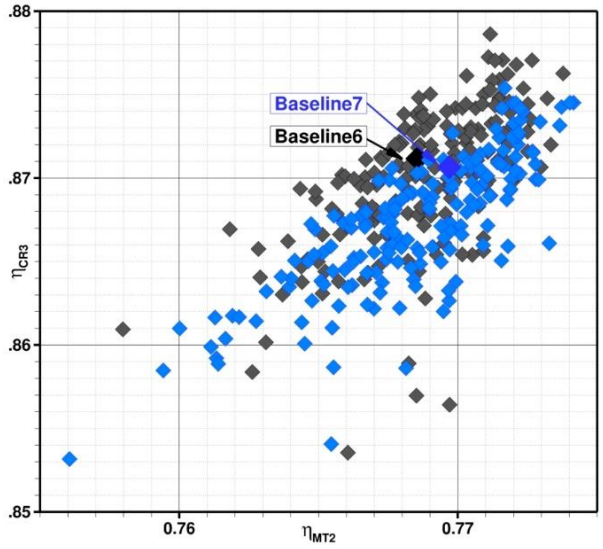


Figure 6 – Results of the DoE and input for the initial surrogate model for the 6- and 7-bladed propellers

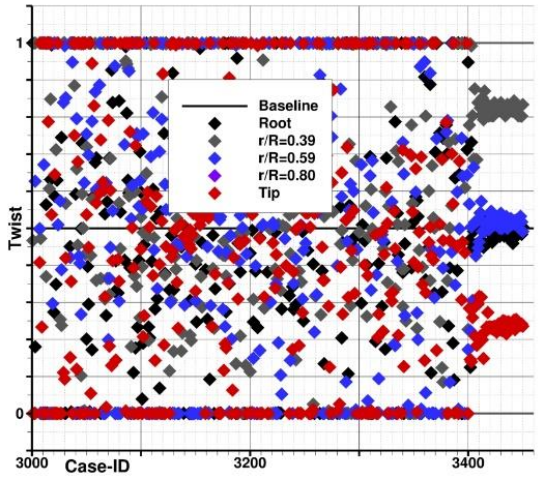
A total of four separate optimization runs are discussed in this paper. The first two are an exploration of the optimization potential of the baseline 6-bladed design in a single-objective SBO at both the cruise and take-off operating points, which were followed by a similar study for an alternative propeller featuring 7 blades, with the baseline/reference blade for both propellers as well as the design space identical for both the 6- and 7-bladed propeller. The maximization of the respective propeller efficiency was the objective in each case. For each of the four runs, the SBO uses a design of experiments (DoE) based on 200 optimized random latin hypercube samples of the overall design space. In all cases, not all of the DoE samples translated into actual successful surrogate model data points, with failures, mostly in the mesh generation step due to complex, unrealistic geometries, eliminating around 30 for each run. Figure 6 plots the results of the RANS simulations in terms of the propulsive efficiencies at both cruise and take-off for the DoE parameter space samples, using black and gray for the 6- and light and dark blue for the 7-bladed propeller cases. The baseline/reference propeller results are marked, which – in-line with expectations – show a slight efficiency degradation at cruise, but a small performance improvement at take-off for the 7-bladed propeller versus the 6-bladed propeller. In both cases however, the DoE indicates that a propeller performance improvement potential exists for both propellers at both operating points. Not unexpected for a propeller design for operation in the subsonic regime – where conventional lower-fidelity design tools have a proven track-record of generating high-performance propeller designs – an improvement of no more than 1 percentage points at either/both operating points appears to be the upper limit based on the DoE results.

Case	Δrms	Δmax
6-Blade Propeller @ CR3	0.223%	0.435%
6-Blade Propeller @ MT2	0.084%	0.168%
7-Blade Propeller @ CR3	0.235%	0.533%
7-Blade Propeller @ MT2	0.071%	0.191%

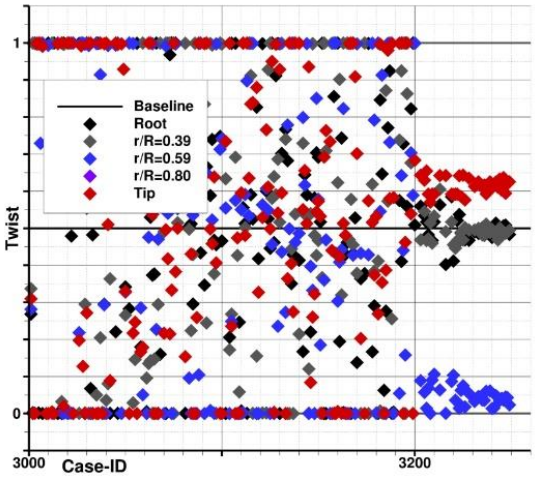
Table 2: Results of the surrogate model tests, using RANS results for 20 random design space samples

An additional 20 design space samples of the design space using Sobol point sampling were then used to test the quality of the resulting surrogate model, by comparing the actual RANS-computed results with those "predicted" by the surrogate model. As listed in table 2, the surrogate model showed average deviations no larger than 0.24% and maximum deviations no larger than 0.54% to the RANS results, indicating that a satisfactory starting point for the SBOs in each case was achieved. As noted in the previous section, the slight blade-foot trailing edge flow separations for the cruise case leads to an increase in uncertainty in the objective function evaluations for that case, which manifest as larger deviations in the surrogate model quality evaluations versus the take-off case.

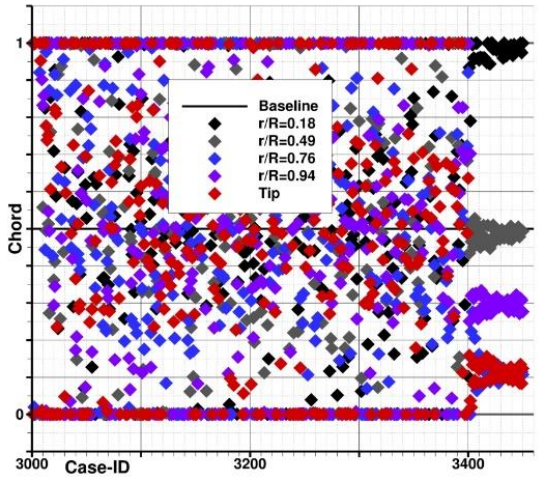
4.1 6-Bladed Propeller SB-Performance Optimization



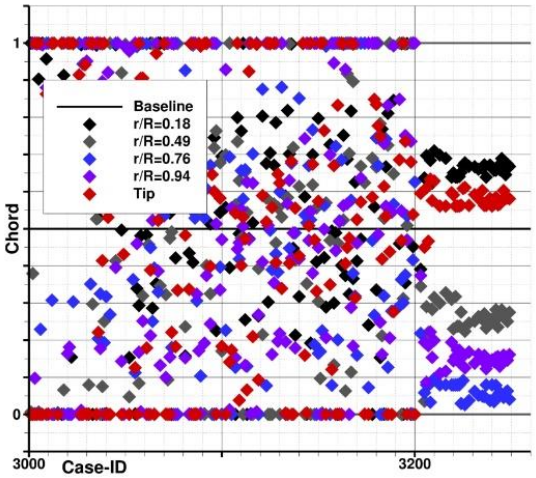
Take-Off SBO, Blade twist parameters



Cruise SBO, Blade twist parameters



Take-Off SBO, Blade chord parameters



Cruise SBO, Blade chord parameter

Figure 7 – Development of the non-dimensional blade twist and chord parameters during the 6-bladed propeller single-objective SBOs

Figure 7 plots the development of the two key design parameters blade twist and airfoil chord length during the two separate single-objective SB-optimization runs for the 6-bladed propeller design study. The parameters space is shown in a non-dimensionalized representation for clarity and comparison.

The SBO was run using an improvement-based infill method for 400 design cycles at take-off and 200 at cruise, followed by 50 additional design iterations with a pure surrogate-value-based infill criterion to obtain a blade shape refinement in a high-trust optimal region of the surrogate model.

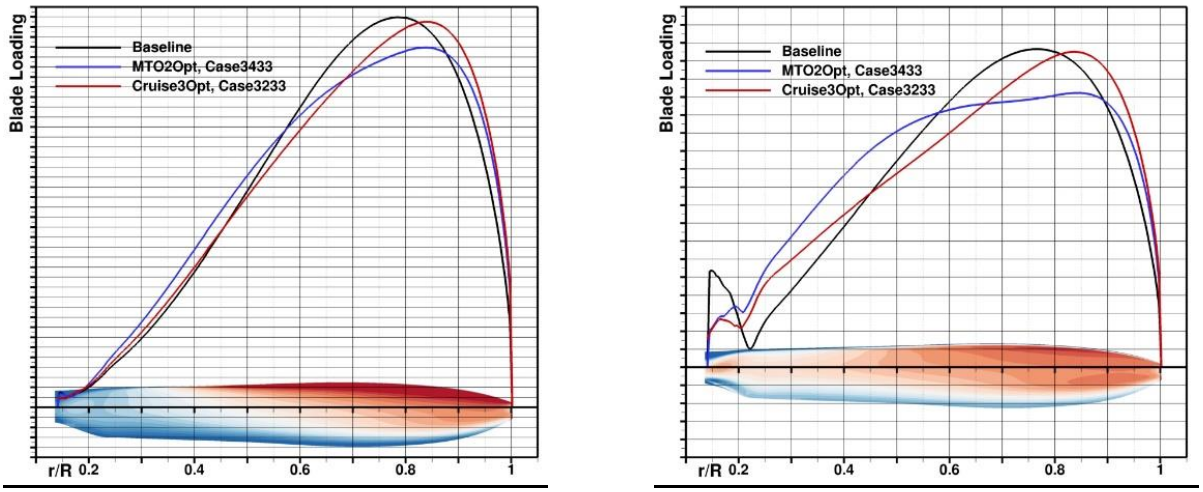


Figure 8 – Comparison of the optimized blade loading distributions versus the baseline blade at the take-off (left) and cruise (right) operating point

As noted earlier, the chord length for the four outboard sections can be scaled up or down by 25% versus the baseline values, meaning the baseline chord length is represented by the solid black line at a value of 0.5 on the y-axis. For the inner-most section, the baseline value is represented by the black line at a value of 1 on the y-axis, as here only a reduction in chord length by 25% versus the baseline value is permitted. For the twist, all sections are free to increase or decrease the airfoil pitch angle by 3 degrees, meaning the baseline value is represented by the solid black line at a value of 0.5 on the y-axis.

For the take-off optimization, the final 50 design refinement cycles indicate a de-twisting of the blade leads to a performance improvement, with a notable increase in the airfoil angle evident at the r/R=0.39 station versus the baseline blade, while a similar magnitude decrease in twist results for the outboard sections. At the same time, the blade chords are reduced near the tip and remain near the baseline values inboard. This leads to a modified blade loading distribution at take-off conditions, plotted for one of the best design iterations of the MT2-optimization as the blue line in figure 8 on the left, where the peak loading at the blade tip is reduced with small increases seen inboard versus the baseline case, shown as the black line in the figure. The propeller efficiency is improved by almost 0.5 percentage points for this blade design, as listed in table 3. The cruise loading distribution, shown on the right in figure 8, also reflects the impact of the blade twist and chord modifications, but this translates to a small degradation of the efficiency at this operating point versus the baseline blade.

	Blade Angle β_{75} [°]	**Efficiency η [%]**	**Thrust Coefficient C_T, [-]**	**Power Coefficient C_P, [-]**
Base6 @ MT2	27.848	76.8557	0.198133	0.223938
Base6 @ CR3	49.355	87.1164	0.180007	0.517865
MT2O C3433 @ MT2	27.368	77.2940	0.199313	0.223994
CR3O C3433 @ CR3	48.421	87.0126	0.178952	0.515445
CR3O C3233 @ MT2	28.700	77.1892	0.199273	0.224253
CR3O C3233 @ CR3	49.840	87.9141	0.181430	0.517224

Table 3: 6-bladed propeller baseline performance metrics in comparison with results from the single-objective optimizations at the take-off and cruise operating points

For the cruise-point optimization on the contrary, the optimal blade design, shown as the red lines in figure 8, retains a high peak loading and shifts it closer to the tip versus the baseline blade. This is achieved by increasing the overall blade twist, with figure 7 showing a small sectional pitch increase at the tip and a very pronounced reduction at the r/R=0.59 station. At the same time blade chord lengths are reduced almost across the complete propeller radius, with a small increase versus the baseline blade only evident at the blade tip. Table 3 shows that cruise performance is improved by around 0.8 percentage points without a take-off performance penalty, which is in fact also improves moderately by 0.3 percentage points.

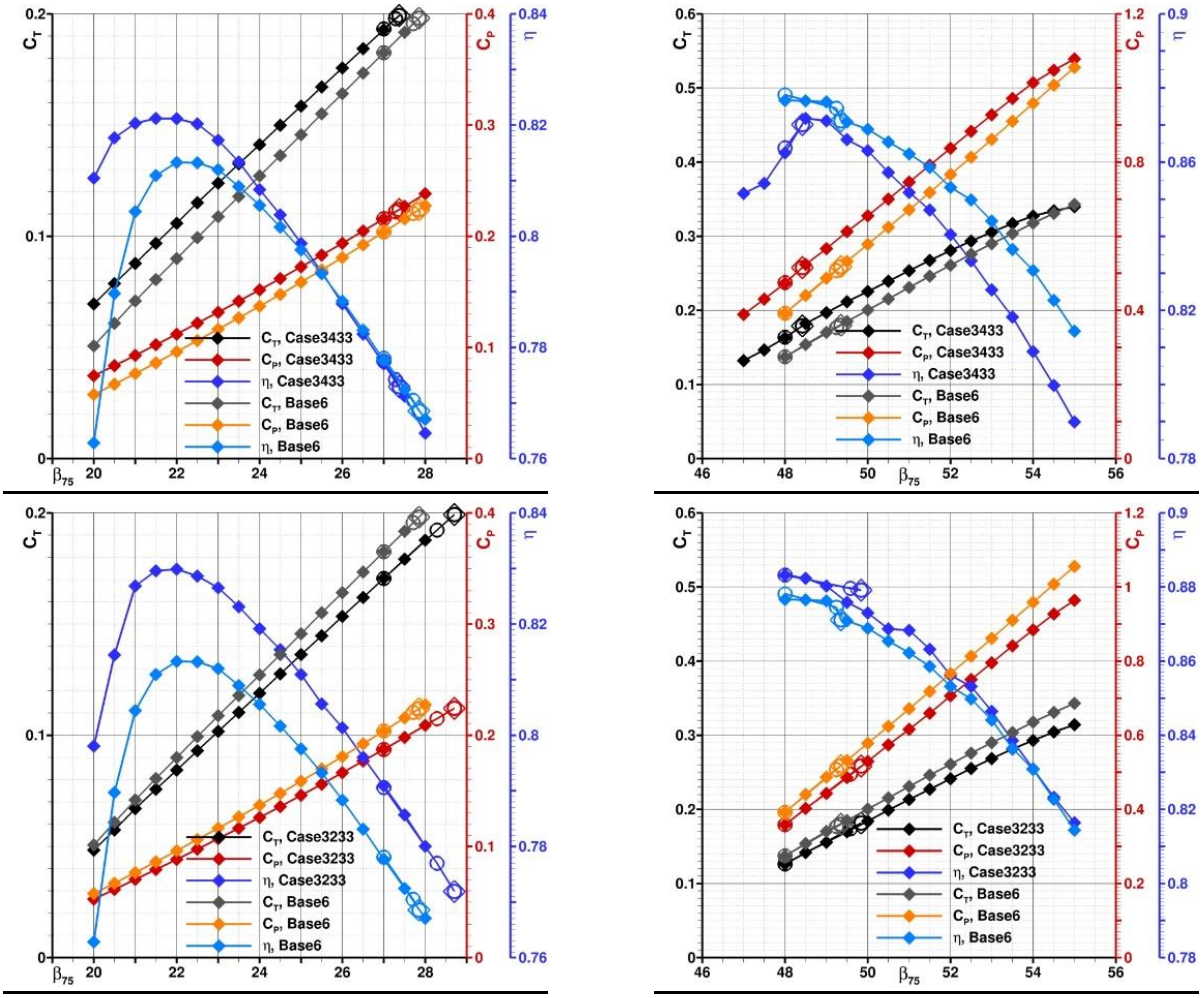


Figure 9 – Overall 6-bladed propeller performance evaluations and comparison with the baseline case for the take-off efficiency (top) and cruise efficiency (bottom) SBO, with take-off performance on the left and cruise performance on the right

Clearly, the slightly higher uncertainty for the cruise condition introduced by the blade foot flow separation is also evident in the overall propeller performance comparisons plotted in figure 9. For this operating point, some discrepancies between the target-power results, plotted using the large diamond symbol in the right-hand side plots, versus the blade-pitch angle sweep results are discernible, that do not show up in the take-off case results on the left in the figure. Nonetheless, and also referring to the surrogate model quality evaluation summarized in table 2, the differences between the optimized and baseline blade results at cruise are significant enough to allow for the noted relative comparisons despite the non-negligible uncertainty in the cruise point RANS evaluations.

These performance improvements highlighted by these single-objective SBOs are in line with the expectations noted earlier based on the DoE results. With the overall goal of the project being a noise-reduction at take-off, figure 10 shows the results of an Ffowcs Williams–Hawkings (FW–H) equation based aeroacoustic evaluation of the DoE cases, provided by the project partners from the Aeroacoustics Department of the DLR Institute of Aerodynamics and Flow Technology. The main

lever to affect the propeller noise emissions for the initial design space chosen here - fixed number of blades, fixed gas turbine operating points and conventional/conservative blade shape design parameters – is the blade loading distribution. As expected, the plots in figure 10 show an inboard shift of the peak loading results in reduced peak noise levels at both take-off (left) and cruise (right). The best-case results for the DoE design candidates indicate a peak noise reduction of only about 1 to 1.5 dB. As the previous discussion has shown, the inboard shift of the blade loading will negatively impact cruise performance and as the aeroacoutic potential identified here is quite small, the decision to switch to a 7-bladed propeller was taken, as the inherent noise reduction potential for this was also substantiated in a coupled RANS/FWH of a baseline 6 and 7-bladed propeller which showed small performance penalties but almost a 3dB noise reduction.

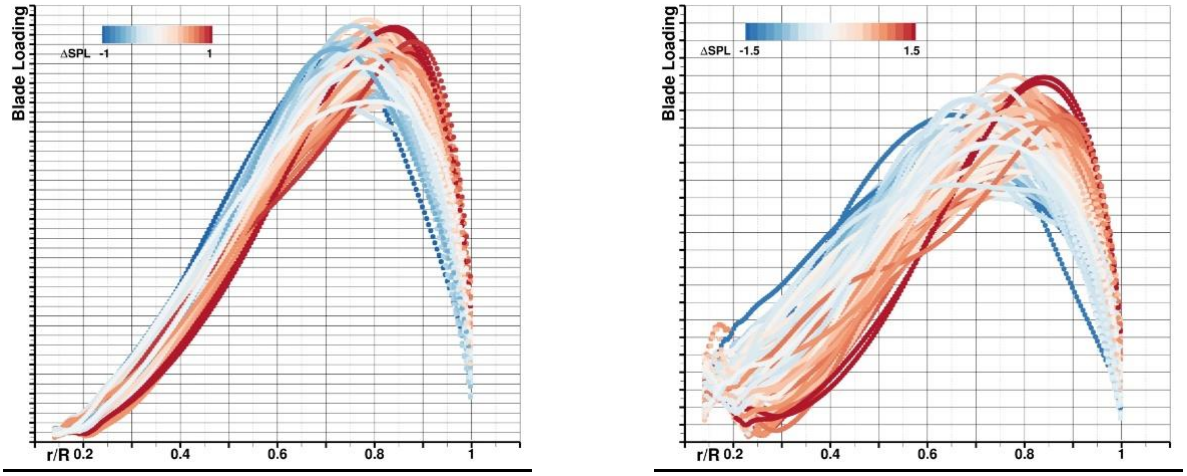


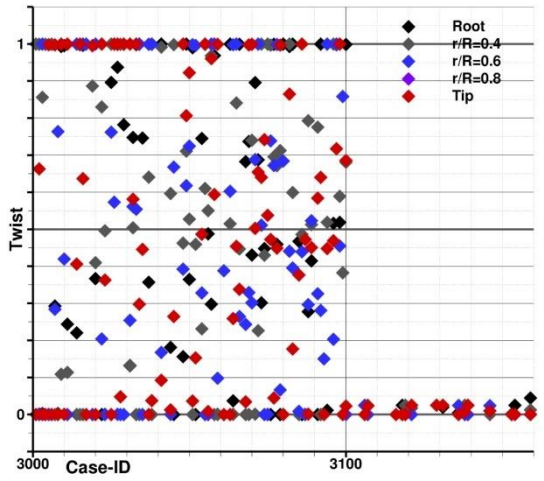
Figure 10 – FW-H-based aeroacosutic analysis of the DoE blade shapes, showing the blade loading distributions colored by the noise deltas versus the baseline 6-bladed propeller for the baseline propeller at the take-off (left) and cruise (right) operating point

4.2 7-Bladed Propeller SB-Performance Optimization

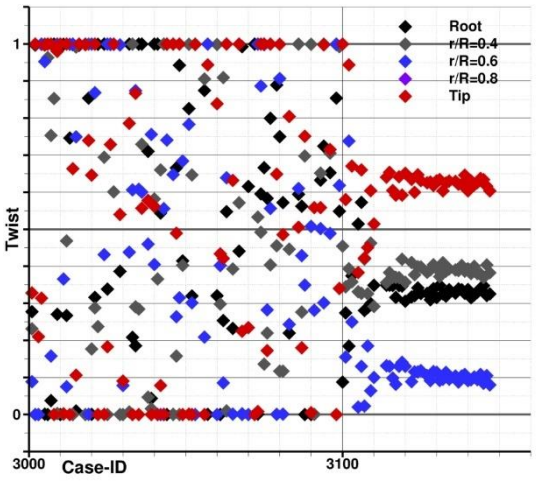
Figure 11 plots the development of the two key design parameters blade twist and airfoil chord length during the two separate single-objective SB-optimization runs for the 7-bladed propeller design study, as discussed previously with respect to figure 7 for the 6-bladed propeller. The parameters space is shown in a non-dimensionalized representation for clarity and comparison. For this design exploration, the SBO was run using an improvement-based infill method for 100 design cycles at take-off and cruise, followed by 50 additional design iterations with a pure surrogate-value-based infill criterion to obtain a blade shape refinement in a high-trust optimal region of the surrogate model.

	Blade Angle β_{75} [°]	Efficiency η [%]	Thrust Coefficient C_T, [-]	Power Coefficient C_P, [-]
Base7 @ MT2	26.766	76.9960	0.196533	0.221802
Base7 @ CR3	48.771	87.0658	0.180658	0.520045
MT2O C3129 @ MT2	27.809	77.4399	0.199789	0.224106
MT2O C3129 @ CR3	49.298	87.2838	0.180966	0.519627
CR3O C3103 @ MT2	28.267	77.0631	0.198983	0.224293
CR3O C3103 @ CR3	49.852	87.7029	0.180853	0.516820

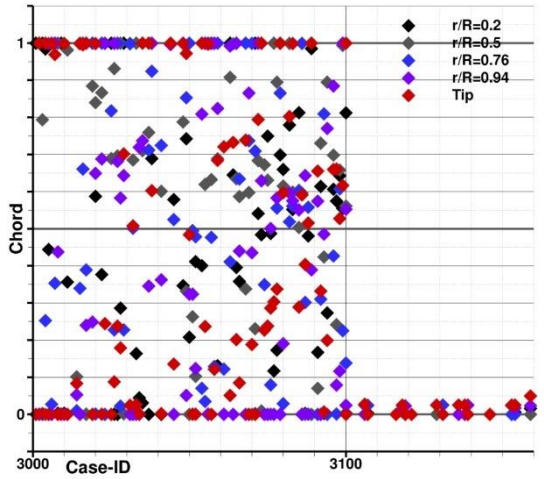
Table 4: 7-bladed propeller baseline performance metrics in comparison with results from the single-objective optimizations at the take-off and cruise operating points



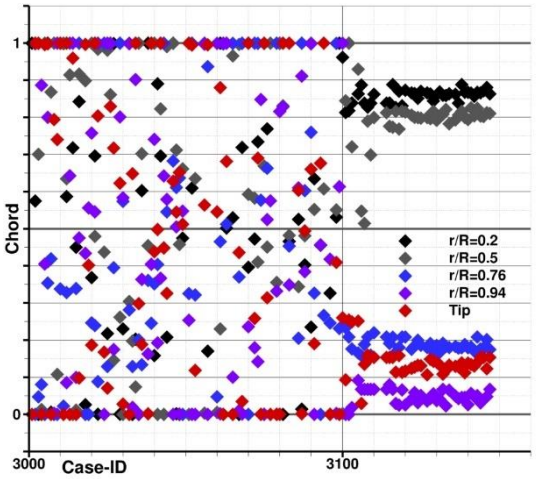
Take-Off SBO, Blade twist parameters



Cruise SBO, Blade twist parameters



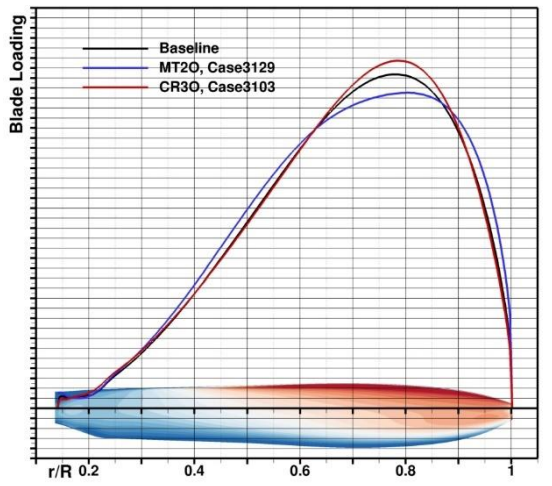
Take-Off SBO, Blade chord parameters



Cruise SBO, Blade chord parameter

Figure 11 – Development of the non-dimensional blade twist and chord parameters during the 7-bladed propeller single-objective SBOs

For the take-off optimization, the final 50 design refinement cycles show that both chord and twist trend towards the minima of the permissible design space values to achieve a performance improvement of nearly 0.5 percentage points versus the baseline 7-bladed propeller, as listed in table 4. This selected representative blade among the MT2-optimized designs also yields a performance improvement at the cruise operating point, besting the baseline 7-bladed propeller by 0.2 percentage points and even still 0.1 percentage points over the baseline 6-bladed propeller.



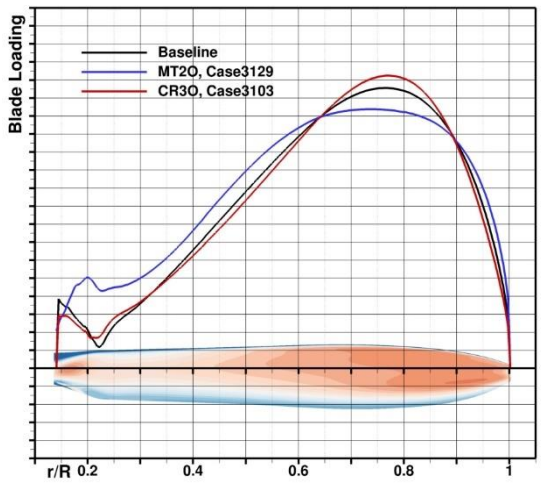


Figure 12 – Comparison of the optimized blade loading distributions versus the baseline blade at the take-off (left) and cruise (right) operating point

Similar to the observations discussed for the 6-bladed propeller, a cruise-optimized blade, as is evident on the right side in figure 12, trends towards an increased tip-loading design by reducing chord lengths almost across the full blade span while a small increase in blade twist at the tip with twist reductions for all inboard sections versus the baseline blade values is introduced. As listed in table 4, this selected optimized blade design delivers an 0.7 percentage point performance improvement over the baseline blade at cruise with a minimal benefit found for this blade at the take-off conditions.

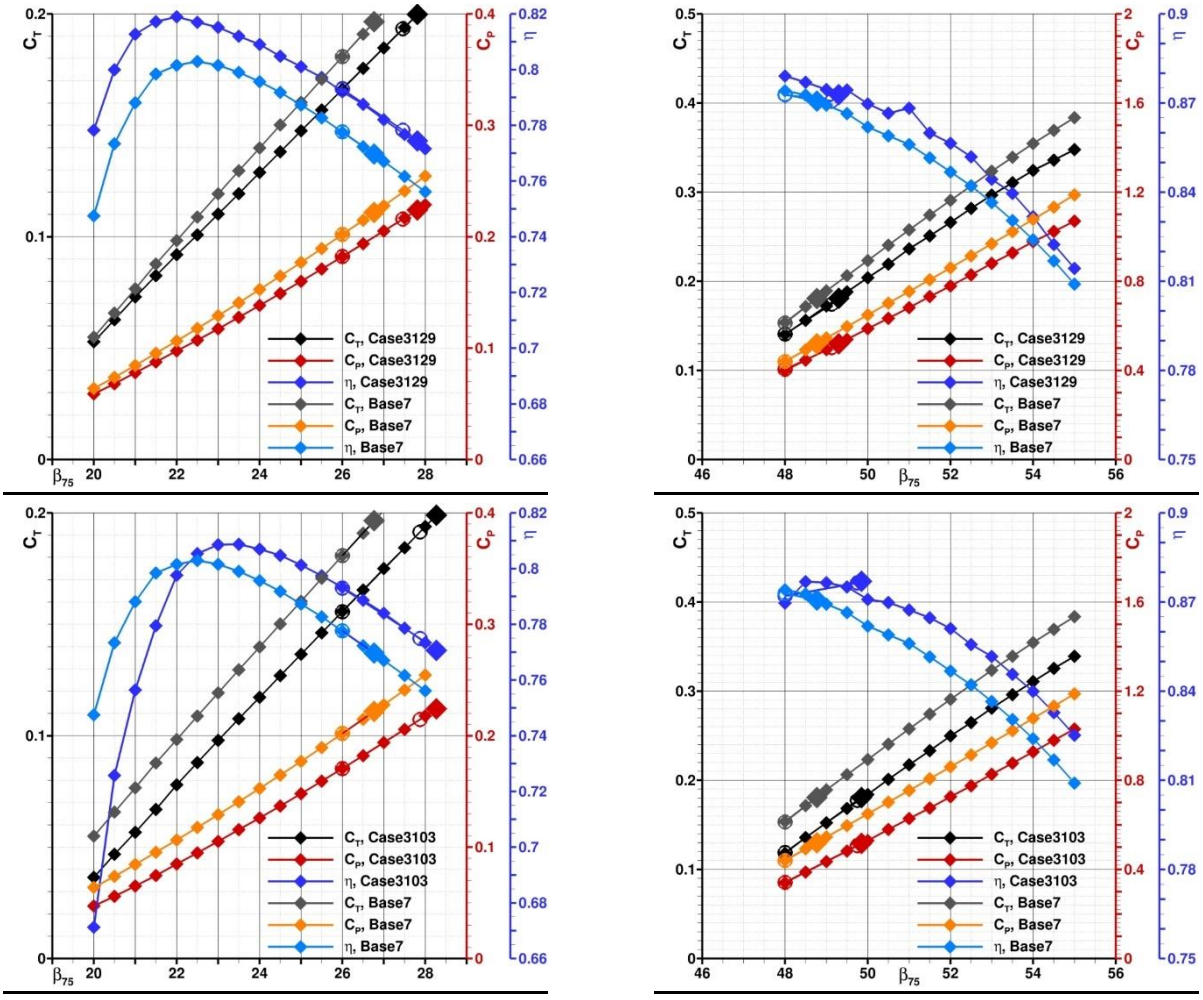


Figure 12 – Overall 6-bladed propeller performance evaluations and comparison with the baseline case for the take-off efficiency (top) and cruise efficiency (bottom) SBO, with take-off performance on the left and cruise performance on the right

Again, the slightly higher uncertainty for the cruise condition introduced by the blade foot flow separation is also evident in the overall propeller performance comparisons plotted in figure 12. For this operating point, some discrepancies between the target-power results, plotted using the large diamond symbol in the right-hand side plots, versus the blade-pitch angle sweep results are discernible, that do not show up in the take-off case results on the left in the figure. Nonetheless, and also referring to the surrogate model quality evaluation summarized in table 2, the differences between the optimized and baseline blade results at cruise are significant enough to allow for the noted relative performance gain comparisons despite the non-negligible uncertainty in the cruise point RANS evaluations

5. Summary and Conclusions

Building on and refining a RANS-based SBO-optimization framework previously applied in contract work, an aerodynamic performance optimization of a propeller targeted at a specific regional turborprop aircraft design mission was performed. Beginning with a generic redesign of the current 6-bladed propeller using typical conceptual blade design tools, single-objective SBOs at the take-off

and cruise operating points were run. These demonstrated that the higher-fidelity RANS aerodynamic analysis used in the SMARTy-based optimization can deliver blade designs that yield performance improvements at both operating conditions of between 0.5 and just under 1 percentage points in the propulsive efficiency. As an analysis of the SBO-results proved that only a marginal improvement in terms of the noise emissions – the main project goal – a similar optimization was done for a 7-bladed propeller, as the increased blade count alone was shown to allow for almost a 3dB noise reduction in an RANS/FWH-based evaluation of the respective baseline propeller designs. The aerodynamic performance SBO of the 7-bladed propeller, with the optimized designs shown in figure 13, demonstrated that propulsive efficiencies at both the cruise and take-off operating point can be obtained that match or exceed those of the current reference 6-bladed propeller.

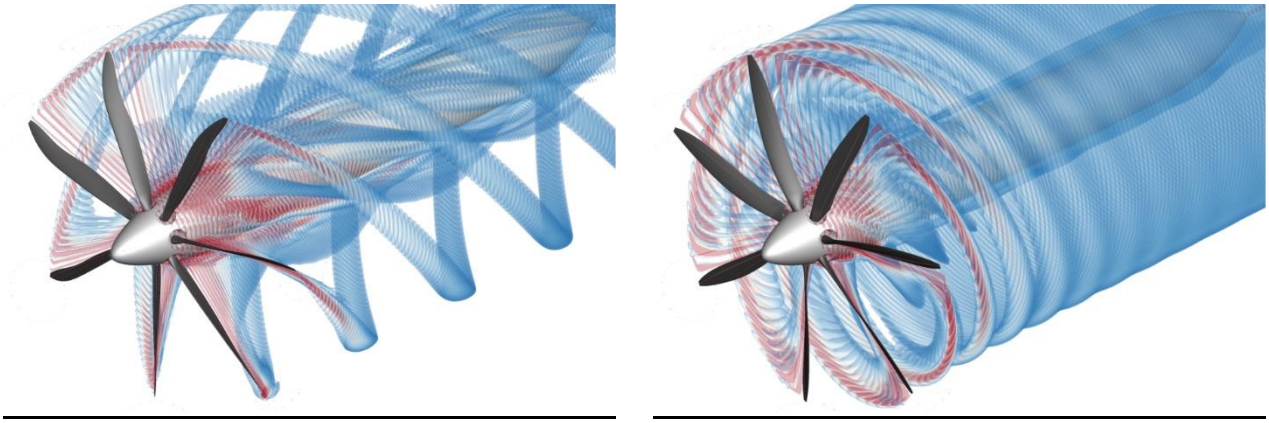


Figure 13 – SBO results, showing blade tip vortices and wakes through vorticity contours, for a cruise-optimized 7-bladed propeller at the cruise (left) and a take-off-optimized 7-bladed propeller at the take-off (right) operating point

The SBO optimization framework has been extended to include an FWH-based aeroacoustic evaluation in a multi-disciplinary approach, which is now being applied towards achieving the PrOpti-project goals of delivering a retrofittable propeller design with notably lower take-off noise emissions without performance penalties across the aircraft design mission operating points.

6. Contact Author Email Address

mailto: arne.stuermer@dlr.de

7. Copyright Statement

The authors confirm that they, and/or their company or organization, hold copyright on all of the original material included in this paper. The authors also confirm that they have obtained permission, from the copyright holder of any third-party material included in this paper, to publish it as part of their paper. The authors confirm that they give permission, or have obtained permission from the copyright holder of this paper, for the publication and distribution of this paper as part of the ICAS proceedings or as individual off-prints from the proceedings.

8. Acknowledgement

The authors gratefully acknowledge the support and contributions of the colleagues in the institutes wind energy group, who developed and made available the Pointwise-based automatic blade meshing tool RoMeO. Furthermore, the support by the SMARTy development team in the institutes numerical methods department $C^2A^2S^2E$ in this effort is much appreciated, with special thanks specifically to the now-former colleague Andrea Garbo. Finally, as core members of the project team, the authors would like to thank the colleagues of the institutes technical acoustics department, Stan Proskurov and Michael Mößner, for their insights and the fruitful collaborations thus far, with their work no doubt being a highlight in upcoming disseminations of the project results.

References

[1] Stuermer, A., “Unsteady CFD Simulations of Contra- Rotating Propeller Propulsion Systems,” *44th AIAA/ASME/SAE/ASEE Joint Propulsion Conference*, No. AIAA 2008-5218, Hartford, CT, USA, 2008.

[2] Stuermer, A. and Yin, J., “Low- Speed Aerodynamics and Aeroacoustics of CROR Propulsion Systems,” *15th AIAA/CEAS Aeroacoustics Conference*, No. AIAA 2009-3134, Miami, FL, USA, 2009.

[3] Stuermer, A. and Yin, J., “Installation impact on pusher CROR engine low speed performance and noise emission characteristics,” *International Journal of Engineering Systems Modelling and Simulation*, Vol. 4, No. 1-2, 2012, pp. 59–68.

[4] Stuermer, A. and Akkermans, R., “Validation of Aerodynamic and Aeroacoustic Simulations of Contra-Rotating Open Rotors at Low-Speed Flight Conditions,” *AIAA Aviation 2014*, No. AIAA 2014-3133, Atlanta, GA, USA, 2014.

[5] Stuermer, A., “Validation of Installation Effect Predictions Through Simulations of CRORs at Low-Speed Flight Conditions,” *AIAA Aviation 2015*, No. AIAA 2015-2886, Dallas, TX, USA, 2015.

[6] Gerhold, T., *Overview of the Hybrid Rans Code TAU*, Vol. 89, Springer Verlag, 2005, pp. 81 – 92.

[7] Spalart, P. and Allmaras, S., “A One-Equation Turbulence Model for Aerodynamic Flows,” Tech. Rep. AIAA 92-0439, 1992.

[8] Langer, S. and Schwoeppe, A.and Kroll, N., “The DLR Flow Solver TAU - Status and Recent Algorithmic Developments,” *52nd Aerospace Sciences Meeting*, No. AIAA 2014-0080, National Harbor, MD, USA, 2014.

[9] Christian Sabater, Philipp Bekemeyer, and Stefan Görtz. Efficient bilevel surrogate approach for optimization under uncertainty of shock control bumps. AIAA Journal, pages 1–15, October 2020. URL: https://doi.org/10.2514/1.j059480, doi:10.2514/1.j059480.

[10] A.I.J Forrester, A. Sóbester, and A.J. Keane. Engineering Design via Surrogate Modelling-A Practical Guide-. John Wiley & Sons, Ltd, 2008.

[11] Ffowcs Williams, J. E., Hawkings, D. L., and Lighthill, M. J., “Sound Generation by Turbulence and Surfaces in Arbitrary Motion,” Philosophical Transactions of the Royal Society of London. Series A, Mathematical and Physical Sciences, Vol. 264, No. 1151, 1969, pp. 321–342.